European Journal of Medicinal Chemistry 211 (2021) 113067

Contents lists available at ScienceDirect

European Journal of Medicinal Chemistry

journal homepage: http://www.elsevier.com/locate/ejmech

Research paper

Conjugation of tacrine with genipin derivative not only enhances effects on AChE but also leads to autophagy against Alzheimer's disease

Rongtian Lin [a], Shuwen Rao [a], Yanbing Li [a], Lei Zhang [a], Liyu Xu [a], Yepu He [a], Zhijun Liu [a], Heru Chen [a, b, c, *]

[a] Institute of Traditional Chinese Medicine and Natural Product, College of Pharmacy, Jinan University, Guangzhou, 510632, PR China
[b] Guangdong Province Key Laboratory of Pharmacodynamic Constituents of TCM and New Drugs Research, Guangzhou, 510632, PR China
[c] International Cooperative Laboratory of Traditional Chinese Medicine Modernization and Innovative Drug Development of Chinese Ministry of Education, School of Pharmacy, Jinan University, Guangzhou, 510632, PR China

ARTICLE INFO

Article history:
Received 8 October 2020
Received in revised form
13 November 2020
Accepted 28 November 2020
Available online 2 December 2020

Keywords:
AChE inhibitor
Alzheimer's disease
Autophagy
Multitarget-directed ligand
Drug design

ABSTRACT

Seven tacrine/**CHR21** conjugates have been designed and synthesized. Compound **8-7** was confirmed as the most active AChE inhibitor with IC_{50} value of 5.8 ± 1.4 nM, which was 7.72-fold stronger than tacrine. It was also shown as a strong BuChE inhibitor (IC_{50} value of 3.7 ± 1.3 nM). **8-7** was clearly highlighted not only as an excellent ChEs inhibitor, but also as a good modulator on protein expression of AChE, p53, Bax, Bcl-2, LC3, p62, and ULK, indicating its functions against programmed cell apoptosis and decrease of autophagy. **8-7** significantly reversed the glutamate-induced dysfunctions including excessive calcium influx and release from internal organelles, overproduction of nitric oxide (NO) and Aβ high molecular weight oligomer. This compound can penetrate blood−brain barrier (BBB). The *in vivo* hepatotoxicity assay indicated that **8-7** was much less toxic than tacrine. Altogether, these data strongly support that **8-7** is a potential multitarget-directed ligand (MTDL) for treating Alzheimer's disease (AD).

1. Introduction

Due to its high incidence, slow progress and high medical costs, Alzheimer's disease (AD) has become a serious neurodegenerative disease affecting human society, especially for the elderly [1]. The occurrence and development of AD are related to the accumulation of abnormal protein β-amyloid protein (Aβ) and tau protein, synaptic loss, oxidative stress, neuronal cell death and inflammation [2]. However, the different mechanisms of AD do not exist in isolation, they are inter-related and interact with each other. For example, amyloid precursor protein (APP) is cleaved by α、β、γ-secretase and aggregated into misfolded Aβ peptides [3], a major pathological hallmark of AD [4]. These misfolded Aβ peptides can act on tau protein to promote neurofibrillary tangles, Ca^{2+} influx to trigger oxidative stress which produces excessive reactive oxygen species (ROS) and reactive nitrogen species (RNS) to cause gene and protein damage [5]. At the same time, oxidative stress factors produced by Ca^{2+} signal can regulate the expression of $A\beta_{1\text{-}42}$ protein [6], and acetylcholinesterase (AChE) can bind with $A\beta_{1\text{-}42}$ to accelerate the aggregation of Aβ [7].

Just like other neurodegenerative diseases, AD has long been viewed as among the most enigmatic and problematic issues in biomedicine [8]. The major basic processes involved are multifactorial in nature, caused by genetic, environmental, and endogenous factors. For such kinds of diseases, "single-molecule, single-target" treatment model cannot achieve good therapeutic effect [9]. On the contrary, the "multi-target-directed ligands" (MTDLs) is a more effective strategy in treating complex diseases because of their ability to interact with the multiple targets thought to be responsible for the disease pathogenesis [10–13].

As the first AChE inhibitor approved for the treatment of AD, tacrine emerges as a popular structure in the design of MTDLs in recent years, because it can inhibit AChE in high potency and has a low molecular weight suitable for modification [14,15]. So far, a lot of MTDLs by combining tacrine with another fragment resulted in

* Corresponding author. Huangpu Avenue West 601, Institute of Traditional Chinese Medicine and Natural Product, College of Pharmacy, Jinan University, Guangzhou, 510632, PR China.
E-mail address: thrchen@jnu.edu.cn (H. Chen).

https://doi.org/10.1016/j.ejmech.2020.113067
0223-5234/

additional activities have been designed and synthesized [15–18]. Unfortunately, serious hepatotoxicity of tacrine limits further use of these compounds [19]. However, it has been disclosed that antioxidants may probably prevent tacrine-induced hepatotoxicity [20,21].

Interestingly, AChE may function by accelerating Aβ formation and could play a role during amyloid deposition in Alzheimer's brain [7]. As a matter of fact, the Aβ deposition in the brain is the primary influence driving AD pathogenesis [22]. This indicates that AD represents the effects of a chronic imbalance between Aβ production and Aβ clearance. Usually, proteins aggregate in the cell are cleared by autophagy, and this mechanism is impaired in AD. It has been demonstrated that autophagy influences the secretion of Aβ to the extracellular space and thereby directly affects Aβ plaque formation [23]. Based on this cognition, we have a bold vision in mind that an autophagy regulator will help to improve AD treatment of an AChE inhibitor.

As an on-going project, we have been working on the possible application of genipin (GP) and its derivatives in the treatment of neurodegenerative diseases [24–27]. It was confirmed that the reduction of the C_6=C_7 double bond in (1*R*)-isopropyloxygenipin (**IPRG001**) or (1*S*)-isopropyloxygenipin led to genipin derivatives **CHR20**, or **CHR21**, respectively, which led to increased flexibility, stability, and enhanced neuronal protection activity [25]. The protection mechanism involved was closely related to the induction of both NO and expressions of anti-oxidative enzymes [28,29]. On the other hand, we noticed that NO does play an important role in regulating autophagy [30]. Taking altogether, this is an appeal to push us to explore whether AD treatment may benefit from the conjugation of tacrine with either **CHR20** or **CHR21**.

Considering that **CHR21** is more active than its isomer **CHR20**, in the present study, **CHR21** was applied as the building scaffold in a series of conjugates with tacrine. The chemistry and biology of these new compounds will be described thereafter.

2. Results

2.1. Chemistry

The novel conjugates consist of a tacrine moiety, a spacer, and a genipin derivative (**CHR21**). Their syntheses were outlined in Scheme 1. The strategy was to prepare the heterocycle firstly, then to introduce the side chain, and finally to combine to **CHR21** moiety. Based on a previously protocol [31], 1,2,3,4-tetrahydro-9-acridone (**1**) was firstly synthesized via the cyclization of anthranilic acid with cyclohexanone. Due to the reason that anthranilic acid is a controlled substance in China, methyl anthranilate was applied as the starting material. This compound was easily hydrolyzed to anthranilic acid using traditional saponification. 9-Chloro-1,2,3,4- tetrahydroacridine (**2**) were then obtained via chlorination of **1** in 89% yield. In order to introduce the spacer, different alkylenediamines (**3-n**, n = 1–7) reacted with **2** leading to 9-aminoalkylamino-1,2,3,4-tetrahydroacridines (**4-n**, n = 1–7) in 65–85% yield. It was found that addition of catalytic amount of KI (10 mol%) shortened the reaction time from 40 h to 8 h with comparative yield.

The synthesis of **CHR21** was referred to our previous work [25]. Firstly, genipin was turned into 1-isopropylgenipin in 96% yield. The resulted product was a mixture of (*1R*)- and (*1S*)-isomers, and was separated by RP-HPLC (COSMOSIL $5C_{18}$-MS-II), where compound **5** was obtained in 63.4% yield. Reduction of **5** with sodium borohydride in the presence of catalytic $NiCl_2$ at −15 °C resulted in chemo- and stereo-selective compound **6**, where 80.3% yield was observed. The absolute configurations at C_1 and C_7 were confirmed by analysis of the coupling constants of C_{7a}-H versus C_1–H and C_7–H, respectively. The C_1–H of **CHR21** displayed a doublet at a δ value of 4.81 ppm, with a coupling constant of 3.2 Hz, which indicates *cis* to C_{7a}-H. Since the configuration at C_{7a} is *S*, the configuration at C_1 is certainly *S*. On the other hand, the C_7–H of **CHR21** displayed a doublet at a δ value of 4.15 ppm, with a coupling constant of 9.2 Hz, which indicates *trans* to C_{7a}-H, implying that the configuration of C_7 is *S*. Oxidation of 10-hydroxyl in **6** with Dess-Martin periodine offered compound **7** in 85.6% yield.

Finally, all the title compounds (**8-n**, n = 1–7) were prepared through reductive amination of **7** with **4-n** (n = 1–7) in 45%–63% yield. The reductant used was sodium borohydride. After silica gel column chromatography, the desired tacrine conjugates were isolated with a high purity degree (>97%).

2.2. In vitro inhibition of ChEs and the structure-activity relationship (SAR)

Compounds **8-n** (n = 1–7), as well as the free amine intermediates **4-n** (n = 1–7) were evaluated for their *in vitro* potential to inhibit cholinesterases (ChEs) including acetylcholinesterase (AChE) and butyrylcholinesterase (BuChE), using tacrine as a positive reference (Table 1). It was indicated that all compounds are potent inhibitors of both ChEs. Just like the tacrine, most of them showed more potent inhibitory activity to BuChE than to AChE. Obviously, the length of the alkyl spacer between **CHR21** and tacrine moiety significantly influenced the ChEs inhibitory activity. It can be seen from Table 1 that compounds **8-1**, **8-6**, and **8-7** with a two-, seven-, and eight-carbon spacer, respectively exhibited more potent AChE inhibitory activity with IC_{50} value of 8.1 ± 1.2, 24.7 ± 1.9, and 5.8 ± 1.4 nM, which was 5.53-, 1.81-, and 7.72-fold stronger than that of tacrine. However, compounds with carbon spacer between 3 and 6 showed weaker AChE inhibitory activity than tacrine itself.

Interestingly, the results of the amine intermediates (**4-n,** n = 1–7) showed a trend consistent with the title compounds, implying that the **CHR21** moiety might not obviously affect the extent of ChE inhibitory activity. Amongst all the tested compounds, **8-1** and **8-7** showed high activity toward both AChE and BuChE. We ascribed the high activity of **8-1** to the enhanced binding affinity of **CHR21** to the catalytic site of ChEs. As for **8-7** with optimal spacer, it is because of the enhanced binding affinity of **CHR21** to the peripheral site of ChEs [31]. This result seems consistent with the previous reports of lipoic acid/tacrine and ferulic acid/tacrine [32,33].

2.3. **8-7** attenuated glutamate-induced injuries to SH-SY5Y cells

In order to evaluate the potential of **8-7** as an agent against Alzheimer disease, an excitotoxicity cell model was set up, where SH-SY5Y cells were treated with 35 mM glutamic acid for 24 h. Since glutamate is the major excitatory neurotransmitter in the mammalian central nervous system, prolonged exposure to glutamate and the associated excessive influx of ions into the cell may arise the injury and death of neurons. These disturbances of the excitatory amino acid system may contribute to the pathogenesis of dementia [34].

As displayed in Fig. 1A and B, treatment of 35 mM glutamate caused cell apoptosis or death (Model group). However, pretreatment of SH-SY5Y cells with 1.25 μM of tacrine (TA), **CHR21**, TA/**CHR21** (in 1:1 mol ratio), and **8-7**, respectively for 4 h attenuated glutamate-induced cells injury. Among them, **8-7** was shown as the most potent to make cells survive from the excitotoxicity impairment, even better than the TA/**CHR21** combination.

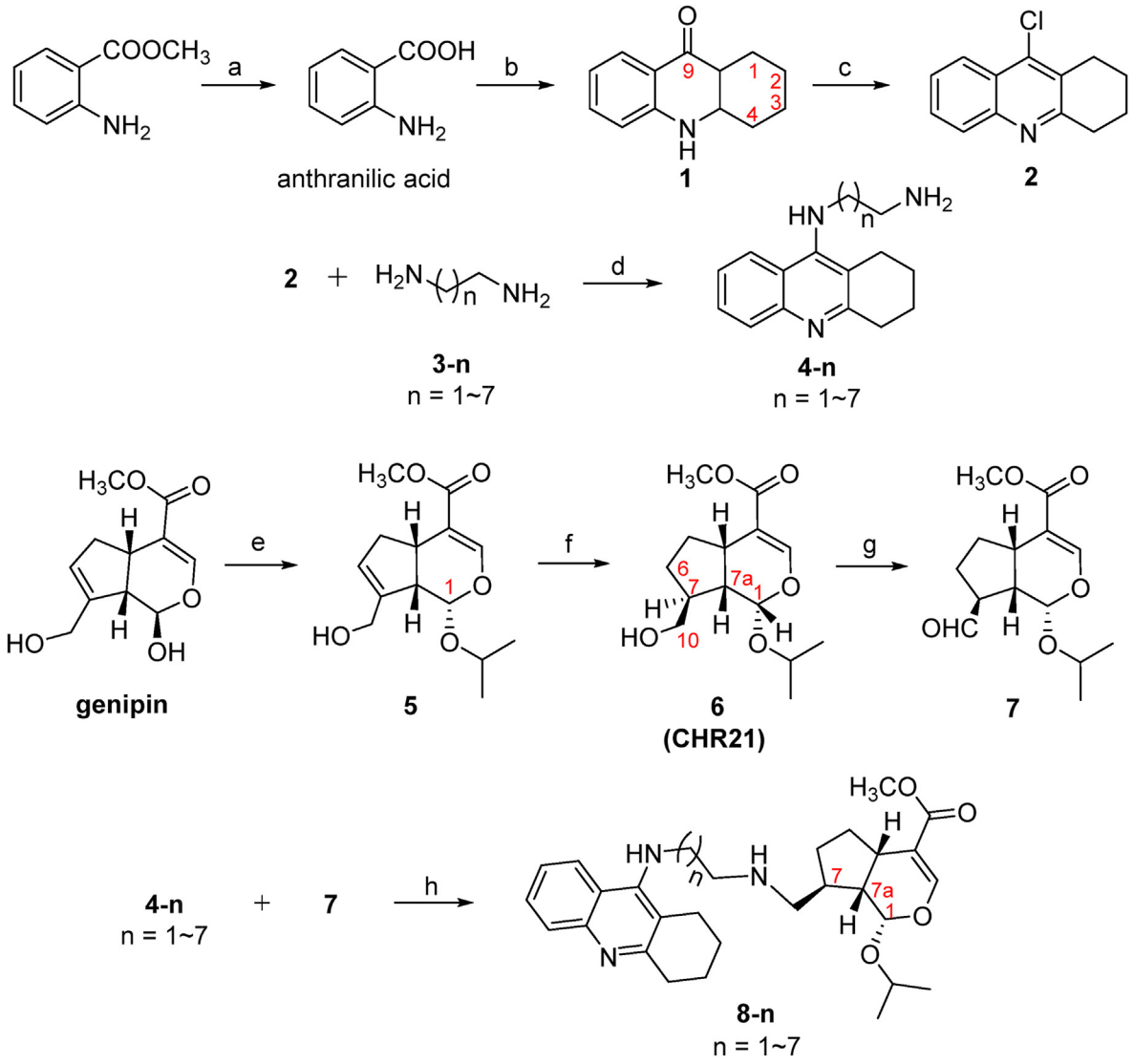

Scheme 1. Design and synthesis of tacrine-**CHR21** hybrids. Reaction conditions: a. sat. NaOH, reflux, 95%; b. cyclohexone/toluent, reflux, 89%; c. $POCl_3$, 120 °C, 91%; d. diamines, KI, 1-pentanol, 160 °C, 65%–85%; e. *i*PrOH, *p*-TsOH, 80 °C, 3 h, 63.4%; f. $NiCl_2 \cdot 6H_2O$, $NaBH_4$, MeOH, −15 °C, 2 h, 80.3%; g. DMP/DCM, r.t., 85.6%; h. $NaBH_4$/MeOH, 0 °C, 45%–63%.

Table 1
IC_{50} values of **4-n** and **8-n** (n = 1–7) against AChE and BuChE.

Compd.	IC_{50} (nM)±SEM[a]		SI[d]
	AChE[b]	BuChE[c]	
4–1	55.2 ± 9.3	13.1 ± 3.8	0.24
4–2	70.3 ± 13.6	5.7 ± 1.3	0.08
4–3	23.6 ± 5.0	6.9 ± 1.2	0.29
4–4	3.6 ± 1.1	5.2 ± 0.8	1.44
4–5	3.2 ± 0.9	1.8 ± 0.6	0.56
4–6	3.5 ± 1.3	2.1 ± 0.8	0.60
4–7	3.7 ± 1.5	1.6 ± 0.5	0.43
8–1	8.1 ± 1.2	5.7 ± 2.1	0.70
8–2	73.2 ± 4.5	35.6 ± 6.3	0.49
8–3	81.4 ± 4.6	43.2 ± 3.8	0.53
8–4	94.6 ± 3.4	57.3 ± 2.6	0.61
8–5	60.6 ± 5.9	27.6 ± 4.5	0.46
8–6	24.7 ± 1.9	11.3 ± 2.4	0.46
8–7	5.8 ± 1.4	3.7 ± 1.3	0.64
tacrine	44.8 ± 6.7	4.8 ± 1.2	0.11

[a] Data is the mean of at least three determinations.
[b] E.C. 3.1.1.7, type VI-S, from Electric Eel.
[c] E.C. 3.1.1.8, from equine serum.
[d] AChE selectivity index = IC_{50}(BuChE)/IC_{50}(AChE).

2.4. ***8-7*** *inhibited glutamate-increased AChE level*

Recent studies have shown that glutamatergic signaling is compromised by Aβ-induced modulation of synaptic glutamate receptors in specific brain regions, paralleling early cognitive deficits [35]. Intriguingly, AChE may function by accelerating Aβ formation and can play a role during amyloid deposition in Alzheimer's brain [7]. Therefore, we postulated that excitotoxicity might have impact on AChE. This prediction was confirmed by data demonstrated in Fig. 2. It can be seen that the treatment of 35 mM glutamic acid to SH-SY5Y cells caused the up-regulation of AChE protein level (Model group). However, pre-treatment of 1.25 μM tacrine alone attenuated this tendency; whilst the conjugate **8-7** showed even stronger activity than tacrine to inhibit this glutamate-increased AChE expression. It was also noticed that pre-treatment of **CHR21** alone displayed no activity.

2.5. ***8-7*** *decreased the glutamate-raised NO and i-NOS levels*

It was demonstrated that excessive activation of glutamate receptors by excitatory amino acids leads to a number of deleterious

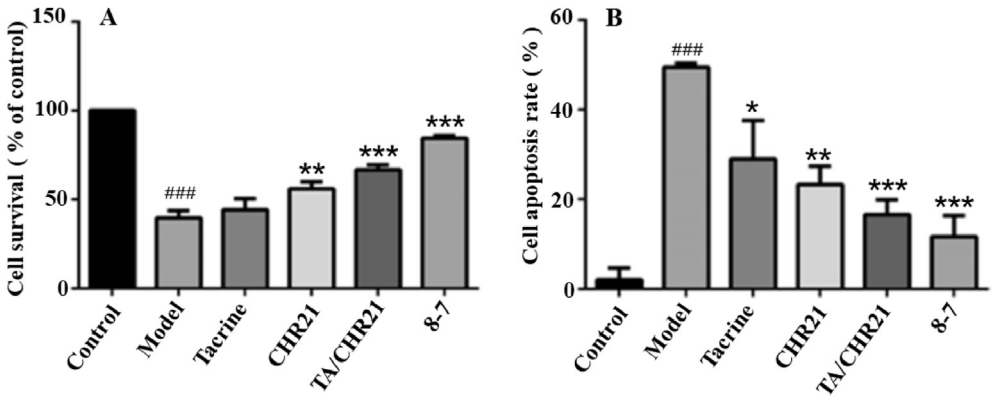

Fig. 1. Protection of **8-7** against glutamate-induced cell injury. (**A**) Cell survival. SH-SY5Y cells were pre-treated with 0.1% DMSO, and 1.25 μM of tacrine (TA), **CHR21**, TA/**CHR21** (in 1:1 mol ratio), **8-7**, respectively for 4 h, then were treated with 35 mM glutamic acid for 24 h. MTT assay was used to determine the cell viability; (**B**) Cell apoptosis rate. SH-SY5Y cells were treated following the procedure described in (**A**). Then the cells were washed with PBS and stained with Annexin-V and PI. The cell apoptosis was detected by flow cytometry. The evaluation of apoptosis is via Annexin V: FITC Apoptosis Detection Kit per manufacture's protocol. The results represent mean ± SD of three separate experiments. $^{###}P < 0.001$ *vs* Control group; $^{*}P < 0.05$, $^{**}P < 0.01$, $^{***}P < 0.001$ *vs* Model group.

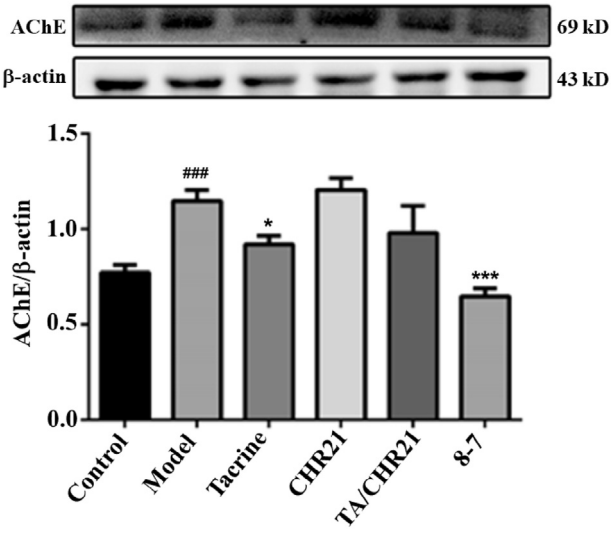

Fig. 2. 8-7 inhibited glutamate-increased AChE level. SH-SY5Y cells were treated following the procedure described in Fig. 1(A). Then the cells were washed and lysed with RIPA buffer. The protein concentration was measured using a BCA protein assay kit. The protein expression was analyzed using Western Blot. The density of each lane was presented as mean ± standard deviation (SD) for at least three individual experiments. Blots were quantified using Image J software. $^{###}P < 0.001$ *vs* Control group; $^{*}P < 0.05$, $^{***}P < 0.001$ *vs* Model group.

consequences, including impairment of calcium buffering, generation of free radicals, activation of the mitochondrial permeability transition and secondary excitotoxicity [36]. The generation of free radicals may result in overproduction of nitric oxide (NO). This prediction was verified in Fig. 3A and B that the treatment of 35 mM glutamic acid to SH-SY5Y cells induced the rise of intracellular NO and inducible NO synthase (*i*-NOS) protein levels (Model group). As a potential anti-AD agent, **8-7** was able to lower the intracellular NO level as well as to down-regulate the *i*-NOS protein level with statistically significant. Moreover, **8-7** was found the most potent agent among tacrine, **CHR21**, and their combination.

2.6. *8-7 lowered the glutamate-elevated Ca^{2+} influx*

Sustained Ca^{2+} influx through glutamate receptor channels is thought to represent a common pathway of neuronal cell death. Excess levels of glutamate in the central nervous system (CNS) can result in elevated intracellular Ca^{2+} levels, which in turn cause a rise in the Ca^{2+} concentration in sensitive organelles such as mitochondria and the endoplasmic reticulum [37]. As shown in Fig. 4A and B, excess levels of glutamate in SH-SY5Y cells did elevate intramolecular Ca^{2+} influx (Model group). More detail, 35 mM glutamate exposure induced an increase in the fluorescence ratio (F340/F380) from 100% in control group to 280% in model group. When the cells were pre-treated with 1.25 μM of tacrine, **CHR21**, TA/**CHR21**, and **8-7**, F340/F380 was reduced from 280% to 145%, 132%, 126%, and 113%, respectively. The reduction of $[Ca^{2+}]_i$ in each group was comparable, but the activity of **8-7** was the most potent.

2.7. *8-7 reduced the glutamate-upregulated level of high molecular weight Aβ oligomer*

According to the amyloid cascade hypothesis, AD pathogenesis is initiated by the overproduction and extracellular deposition of Aβ and the intracellular deposition of neurofibrillary tangle (NFT). These depositions serve as initiating factors for multiple neurotoxic pathways, which may include excitotoxicity, oxidative stress, energy depletion, inflammation and apoptosis [38]. In turn, excitotoxicity might induce the overproduction of Aβ. This deduction was verified by the fact shown in Fig. 5. It was displayed that exposure of excessive glutamate (35 mM) raised the level of high molecular weight Aβ oligomer (42 kD). The protein ratio to β-actin was elevated from 0.75 in Control group to 1.4 in Model group. When the cells were pre-treated with 1.25 μM of tacrine, **CHR21**, TA/**CHR21**, and **8-7**, the ratio was reduced from 1.4 to 1.2, 1.1, 0.9, and 0.7, respectively. The result of tacrine group was showed without statistically significant. Excitingly, the activity of **8-7** was better than that of either **CHR21** or the combination. It was the most active compound in down-regulating toxic Aβ oligomer.

2.8. *8-7 down-regulated the glutamate-raised p53 level*

No doubt, overactivation of glutamate receptors impairs cellular calcium homeostasis and activates NO synthesis, generates free radicals and causes programmed cell death [39]. As an apoptotic protein, p53 is involved during programmed cell death. It was shown in Fig. 6 that exposure of SH-SY5Y cells to 35 mM glutamate induced a rapid increase in p53 protein level, whereas the protein ratio to β-actin was elevated from 0.85 in Control group to 1.28 in Model group. When the cells were pre-treated with 1.25 μM of

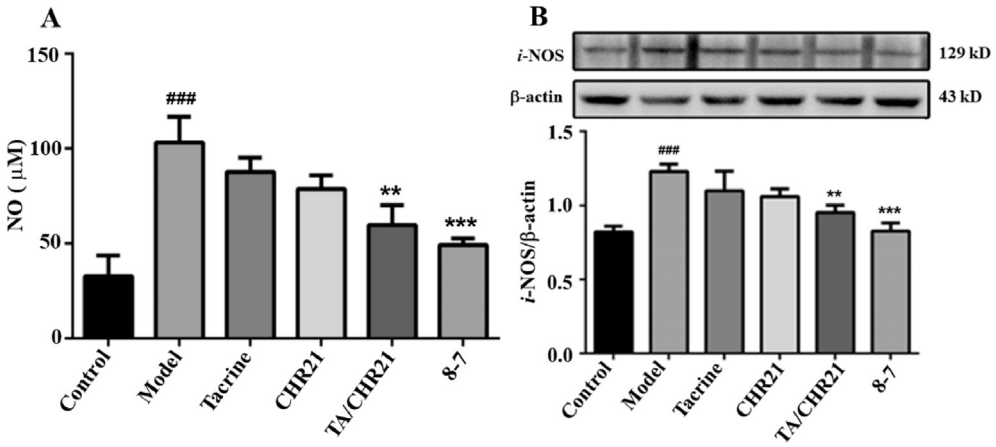

Fig. 3. **8-7** decreased glutamate-rised NO and i-NOS levels. (**A**) NO level. SH-SY5Y cells were treated following the procedure described in Fig. 1(A). Then the cells were washed and lysed with RIPA buffer. The levels of intracellular NO were determined by the colorimetric assay using the nitrite colorimetric assay kit (Beyotime, China); (**B**) *i*-NOS level. The protein concentration was measured using a BCA protein assay kit. The protein expression was analyzed using Western Blot. The density of each lane was presented as mean ± standard deviation (SD) for at least three individual experiments. Blots were quantified using Image J software. $^{###}P < 0.001$ *vs* Control group; $^{**}P < 0.01$, $^{***}P < 0.001$ *vs* Model group.

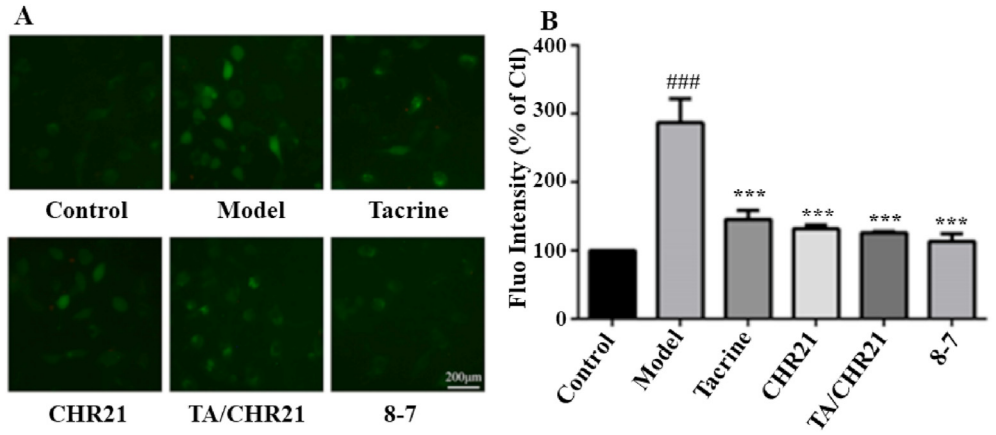

Fig. 4. **8-7** lowered the glutamate-elevated Ca^{2+} influx. (**A**) Photograph of Fura-3/AM dyed cells. SH-SY5Y cells were treated following the procedure described in Fig. 1(A). Afterwards, the cells were trypsinized, pelleted, resuspended in medium and incubated with 5 μM Fura-3/AM in PBS containing 1.3 mM $CaCl_2$ for 40 min at 37 °C and then washed twice to remove any extracellular dye. Then the cells were submitted to fluorescence microscope for photograph. (**B**) Fluorescence intensity of intramolecular Ca^{2+}. All the dyed cells were submitted to a flow cytometry (BD FACS Calibur, Franklin Lakes, CA, USA) for fluorescence detection. Excitation wavelength was 340/380 nm; emission wavelength was 510 nm. The fluorescence ratio (F340/F380) was calculated as an indicator of $[Ca^{2+}]_i$. The intensity of each lane was presented as mean ± standard deviation (SD) for at least three individual experiments. $^{###}P < 0.001$ *vs* Control group; $^{***}P < 0.001$ *vs* Model group.

tacrine, **CHR21**, TA/**CHR21**, and **8-7**, the ratio was reduced from 1.4 to 1.1, 1.08, 1.16, and 0.72, respectively. Again, the activity of conjugate **8-7** was confirmed the most potent agent. Intriguingly, the combination showed a bit less active than both monomers.

2.9. *8-7 attenuated the glutamate-influenced LC3 and p62 protein levels*

Excessive uptake of calcium or generation of ROS induces activation of the mitochondrial permeability transition. And low-intensity stress can cause depolarization of mitochondria leading to autophagy, which in turn selectively removes damaged mitochondria as a cytoprotective mechanism [40]. As an autophagosome marker, the microtubule-associated protein 1A/1B-light chain 3 (LC3) has been used to monitor autophagy. During autophagy, a cytosolic form of LC3 (LC3-I) is conjugated to phosphatidylethanolamine to form LC3-phosphatidyl- ethanolamine conjugate (LC3-II), which is recruited to autophagosomal membranes. The protein p62, which binds ubiquitin and LC3, is a selective substrate for autophagy. It regulates the formation of protein aggregates. In the current studies, it was disclosed that exposure of SH-SY5Y cells to 35 mM glutamate decreased LC3-II/LC3-I ratio (Fig. 7A, model group); in the meantime, it increased p62 protein level (Fig. 7B, model group). Both results consistently indicated the reduction of autophagy. Interestingly, pre-treatment of 1.25 μM **8-7** reversed this glutamate-influenced tendency. It raised the LC3-II/LC3-I ratio and down-regulated p62 protein level, both consistently implied the augment of autophagy.

2.10. *8-7 elevated the phosphorylation levels of ULK*

Since **8-7** reversed the glutamate-influenced LC3 and p62 protein levels, it may probably have an impact on Unc-51 like kinase (ULK) 1 and 2. As we know, ULK1 and 2 are multifunctional proteins with roles in autophagy, neurite outgrowth, and vesicle transport. The ULK1 balance is very important in autophagy modulation.

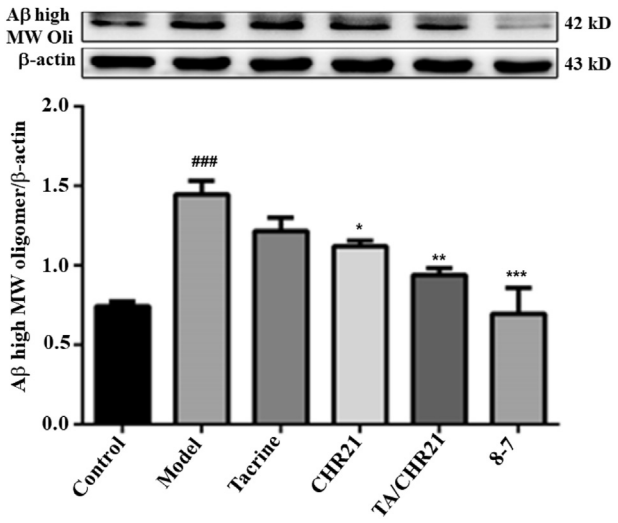

Fig. 5. 8-7 reduced the glutamate-upregulated level of high molecular weight Aβ oligomer. SH-SY5Y cells were treated following the procedure described in Fig. 1(A). Then the cells were washed and lysed with RIPA buffer. The protein concentration was measured using a BCA protein assay kit. The protein expression was analyzed using Western Blot. The density of each lane was presented as mean ± standard deviation (SD) for at least three individual experiments. Blots were quantified using Image J software. $^{###}P < 0.001$ *vs* Control group; $^{*}P < 0.05$, $^{**}P < 0.01$, $^{***}P < 0.001$ *vs* Model group.

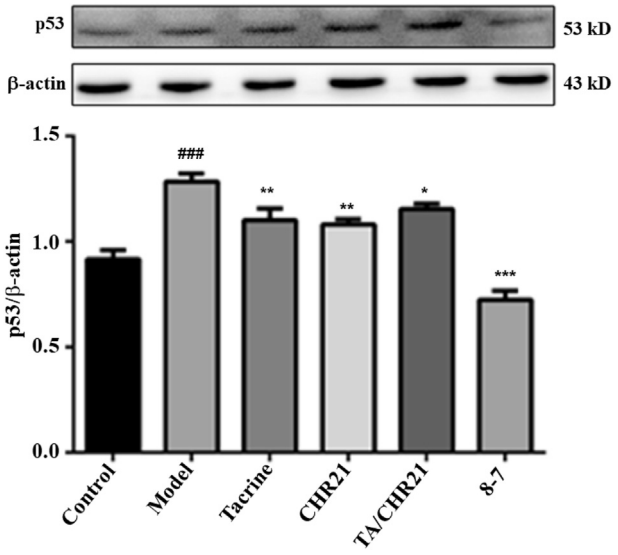

Fig. 6. 8-7 down-regulated the glutamate-raised p53 protein level. SH-SY5Y cells were treated following the procedure described in Fig. 1(A). Then the cells were washed and lysed with RIPA buffer. The protein concentration was measured using a BCA protein assay kit. The protein expression was analyzed using Western Blot. The density of each lane was presented as mean ± standard deviation (SD) for at least three individual experiments. Blots were quantified using Image J software. $^{###}P < 0.001$ *vs* Control group; $^{*}P < 0.05$, $^{**}P < 0.01$, $^{***}P < 0.001$ *vs* Model group.

Therefore, we investigated the influence of **8-7** on ULK. As shown in Fig. 8, exposure of SH-SY5Y cells to 35 mM glutamate down-regulated phospo-ULK/ULK protein ratio, implying the reduction of autophagy. However, pre-treatment of 1.25 μM **8-7** significantly elevated the phospo-ULK/ULK protein ratio, indicating the increase of autophagy. It can be seen from Fig. 8 that the activity of tacrine/**CHR21** combination was far less than that of **8-7**.

2.11. Blood–brain barrier (BBB) permeability assay

Penetration of the blood–brain barrier (BBB) is a critical factor for successful CNS drugs. To determine the BBB penetration of the candidate, the parallel artificial membrane permeability (PAMPA) assay was employed, which was initially established by Di et al. [41]. In the current experiment, 7 commercial drugs through a lipid extract of porcine brain were determined using a mixture of PBS and ethanol in the ratio of 70:30 (Table S1, Supporting Information). A plot of experimental data versus reported values produced the linear correlation *Pe* (exp) = 1.1719*Pe*(bibil.)-0.0221 (R^2 = 0.9404) (Fig. S6). According to this equation and taking into account the described limits by Di et al. for BBB permeation, we determined that compounds with permeability above 4.67 × 10^{-6} cm/s penetrate into the CNS by passive diffusion. Based on this assay, the permeability of **8-7** was found (4.92 ± 0.67) × 10^{-6} cm/s, indicating good permeability to penetrate BBB.

3. Discussion

In the present investigations, we confirmed that incorporation of **CHR21** with tacrine through a propriate spacer did enhance the binding affinity with AChE. As the most optimal candidate, **8-7** showed 7.72-fold stronger activity than tacrine itself. Furthermore, cytotoxicity of **8-7** against SH-SY5Y cells was far less than that of tacrine (Fig. S1). It is nontoxic even at the dose of 100 μM.

As we know, excitatory amino acids serve as the major excitatory neuro-transmitters in the cerebral cortex and hippocampus. Neurons containing excitatory amino acids play crucial roles in psychological functions such as learning and memory. Therefore, we set up an excitotoxic cell model to evaluate their potential against Alzheimer's disease. It was found that exposure of SH-SY5Y cells to 35 mM glutamate caused cell death involving excessive calcium influx and release from internal organelles (Fig. 4), NO generation (Fig. 3A), Aβ high MW oligomer accumulation (Fig. 5), and oxyradical production (Fig. S2). In all cases, the conjugate **8-7** showed the best activity to reverse the glutamate-elevated levels of all these indications.

It has been recognized nowadays that acetylcholine is widely distributed in the nervous system and has been implicated to play a critical role in cerebral cortical development, cortical activity, controlling of cerebral blood flow, and sleep-wake cycle as well as in modulating cognitive performance and learning and memory processes [42]. No doubt, overactivation of AChE causes the loss of cholinergic neurons, consequently leading to AD. In the current study, we noticed that exposure of SH-SY5Y cells to 35 mM glutamate up-regulated AChE protein level (Fig. 2). Interestingly, as a clinical AChE inhibitor, tacrine was capable of attenuating the level of AChE, while the conjugate **8-7** showed more active than tacrine. The monomer **CHR21** was found no activity.

There is accumulating evidence that soluble amyloid-β (Aβ) oligomers, rather than amyloid fibrils, are the principal pathogenic species in AD [43,44]. Overactivation of glutamate receptors does increase the level of Aβ high MW oligomer, implying the close relation between AD and excitotoxicity. As a clinical anti-AD agent, tacrine showed a tendency to down-regulate the level of Aβ high MW oligomer without statistically significant (Fig. 5). However, **8-7** significantly decreased this oligomer level. Consistently, overactivation of glutamate receptors also elevated the protein level of beta-site amyloid precursor protein–cleaving enzyme 1 (BACE1) (Fig. S3). This enzyme is essential for the generation of Aβ peptide in AD. Interestingly, **8-7** significantly down-regulated BACE1 protein level; while tacrine did not have this function. All these data indicate that **8-7** is a more potent agent in the treatment of AD than tacrine.

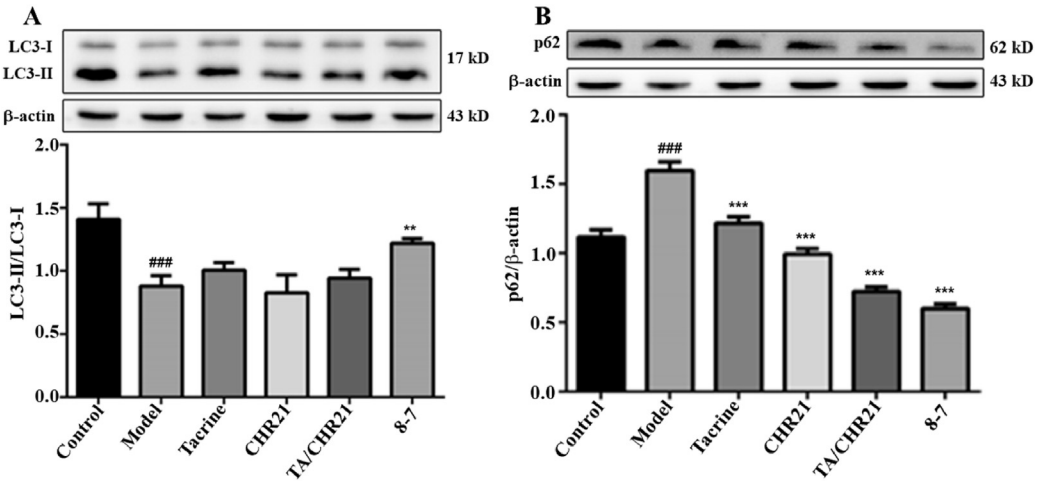

Fig. 7. **8-7** attenuated the glutamate-influenced LC3 and p62 protein levels. (**A**) **8-7** up-regulated the glutamate-reduced LC3-II/LC3-I ratio; (**B**) **8-7** attenuated the glutamate-increased p62 protein level. The protein expression was analyzed using Western Blot. The density of each lane was presented as mean ± standard deviation (SD) for at least three individual experiments. Blots were quantified using Image J software. $^{###}P < 0.001$ *vs* Control group; $^{**}P < 0.01$, $^{***}P < 0.001$ *vs* Model group.

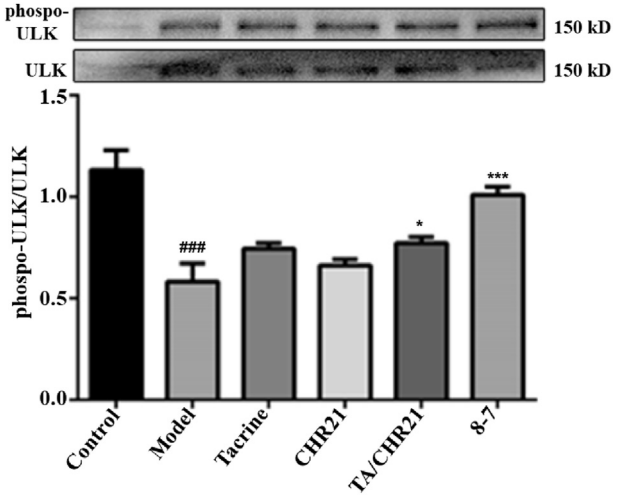

Fig. 8. **8-7** reversed the glutamate-decrased phospo-ULK/ULK ratio. SH-SY5Y cells were treated following the procedure described in Fig. 1(A). Then the cells were washed and lysed with RIPA buffer. The protein concentration was measured using a BCA protein assay kit. The protein expression was analyzed using Western Blot. The density of each lane was presented as mean ± standard deviation (SD) for at least three individual experiments. Blots were quantified using Image J software. $^{###}P < 0.001$ *vs* Control group; $^{*}P < 0.05$, $^{***}P < 0.001$ *vs* Model group.

We did notice that programmed cell death (apoptosis) cascades were engaged in excitotoxicity. Exposure of SH-SY5Y cells to 35 mM glutamate induces a rapid increase in mRNA and protein levels of p53 and Bax (Fig. 6 and Fig. S4). These apoptotic proteins induce mitochondrial membrane permeability changes resulting in the activation of proteases, such as caspase-3 (Fig. S5). Pre-treatment with 1.25 μM tacrine, **CHR21**, TA/**CHR21**, and **8-7**, respectively, prevented glutamate-induced increase in p53 and Bax expression and maintains Bcl-2 in an elevated state. The down-regulation of p53 and Bax implied the decrease of cell apoptosis. This was consistent with the down-regulated level of phospo-Caspase 3 (Fig. S5). Again, **8-7** was displayed as the most potent agent amongst them.

Nowadays, it is well known that autophagy is a lysosomal degradative process used to recycle obsolete cellular constituents and eliminate damaged organelles and protein aggregates. It is close related to neurodegenerative diseases. Recent evidence shows that autophagy impairment is a pathogenic role in several major neurodegenerative diseases [45]. This provides a strong rationale for developing therapeutics to modulate autophagy in these disorders. In the current research, we found that exposure of SH-SY5Y cells to 35 mM glutamate reduced autophagy, where LC3-II/LC3-I ratio and phospo-ULK level was decreased, and p62 level was elevated (Fig. 7A and B and Fig. 8). However, pre-treatment of **8-7** consistently reversed glutamate-induced tendencies, indicating the raise of autophagy with statistically significant. Once again, **8-7** was shown as the most active modulator to autophagy, compared to both monomers and the combination. This implied that **8-7** can alleviate Alzheimer's disease by the adjustment of autophagy.

Fortunately, incorporation of **CHR21** to tacrine does reduce the hepatotoxicity caused by tacrine. As shown in Fig. S7, tacrine induced significant hepatotoxicity indicated by increased activity of both aspartate aminotransferase (AST) and alanine aminotransferase (ALT) at 24, and 36 h, respectively; while compound **8-7** did not alter these parameters from 0 to 72 h. In the meantime, an increase in the number of inflammatory cells in portal fields and a large area of necrosis and distinct fatty degeneration of the hepatocytes were observed after tacrine treatment. However, only minor morphological changes were found after the administration with 8-7 (Fig. S8). We attributed this to the enhanced antioxidative capacity induced by **CHR21** [25].

4. Conclusion

In summary, a novel series of tacrine/**CHR21** conjugates has been designed and synthesized. Their biological activities on inhibition of ChEs and protection on glutamate-induced cell impairment were evaluated. It was found that when tacrine was conjugated with **CHR21** through an 8-carbon chain, the resulted candidate (compound **8-7**) showed the most active inhibitory effect on AChE, which was 7.72-fold stronger than tacrine.

Exposure of SH-SY5Y cells to 35 mM glutamate elevated cell death including programmed cell apoptosis, and protein levels of AChE, *i*-NOS, Aβ high MW oligomer, p53, Bax, and p62; Whilst in the meantime, down-regulated the ratios of LC3-II/LC3-I and phospo-ULK/ULK. It also induced excessive calcium influx and release from internal organelles, raised NO production.

Interestingly, pretreatment of 1.25 μM **8-7** significantly reversed all these glutamate-induced dysfunctions. It was confirmed the most potent candidate if compared to tacrine, **CHR21**, and TA/**CHR21** combination. Furthermore, **8-7** showed the BBB permeability by passive diffusion, and it did not show signs of hepatotoxicity, which was much safer than tacrine.

Altogether, these data strongly support that **8-7** is a reliable and potent drug candidate for treating AD. It was clearly disclosed as an excellent AChE inhibitor and protein regulator, as well as a good protein modulator against *i*-NOS, p53, Bax, LC3, p62 and ULK.

5. Experimental section

5.1. General methods for chemistry

All reagents and solvents were used as purchased from commercial sources or indicated otherwise. Flash chromatography was performed using silica gel (300 mesh). All reactions were monitored by TLC, using silica gel plates with the fluorescence F_{254} displayed by UV light visualization. ^{1}H NMR and ^{13}C NMR spectra were recorded on a Bruker AV-400 spectrometer or Bruker AV-300. Coupling constants (*J*) are expressed in Hertz (Hz). Chemical shifts (δ) of NMR are reported in parts per million (ppm) units relative to an internal control (TMS). Low resolution ESI-MS data were recorded on a Finnigan LCQ Advantage MAX mass spectrometer and high resolution ESI-MS data on an Applied Biosystems Q-STAR Elite ESI-LC-MS/MS mass spectrometer. The purity of the compounds was determined by reverse phase high performance liquid chromatography (HPLC) analysis to be >95%. HPLC was performed on either LC-100 liquid chromatograph equipped with a tunable LC-100 UV detector (Shanghai Wufeng Inc., China) or Agilent 1200 series liquid chromatograph equipped with an Agilent 1200 Series UV detector (Agilent Technologies, USA). The columns used were Cosmosil 5C_{18} (Nacalai Tesque Inc., Japan) for general purification. A flow rate of 1.0 mL/min was used with mobile phase of MeOH in H_2O with 0.1% modifier (ammonia or trifluoroacetic acid, *v/v*).

The synthesis of compd. **4-n** (**n** = **1~7**) started from methyl anthranilate followed a procedure reported in one of our previous works [46]. The purity of each alkylenediamine was more than 95.0%. Whilst the preparation of compd. **6** (**CHR21**) was carried on based on the process shown in another of our early works [25].

5.1.1. Methyl (1S,4aS,7S,7aS)-7-formyl-1-isopropoxy-1,4a,5,6,7,7a-hexahydro- cyclopenta[c]pyran-4-carboxylate (7)

To a 25-mL round-bottom flask, compd. **6** (121.6 mg, 0.45 mmol) was dissolved in 8.0 mL dried dichloromethane (DCM). Then Dess-Marin reagent (384.5 mg, 0.90 mmol) was added portion by portion within 0.5 h. The suspension mixture was kept stirring at r. t. for 6 h, and then was put over ice-batch for 0.5 h. Filtration was carried on. The residues were washed with DCM. All the filtrates were combined, dried over anhydrous Na_2SO_4. Removal of solvent was then carried on by rotating distillation. The residues were submitted to flash column liquid chromatography for purification applying petroleum/ethyl acetate (1:1 in *V*:*V*) as eluent, offering white oil 103.4 mg in 85.6% yield. ^{1}H NMR (300 MHz, $CDCl_3$) δ: 9.83 (d, J = 5.1 Hz, 1H), 7.41 (s, 1H), 5.43 (d, J = 3.3 Hz, 1H), 3.97−3.92 (m, 1H), 3.72 (s, 3H, $-OCH_3$), 2.82−2.73 (q, J = 8.4 Hz, 1H), 2.50−2.40 (m, 1H), 2.34−2.28 (m, 1H), 2.17 (dd, J = 9.1, 3.3 Hz, 1H), 1.79−1.60 (m, 2H), 1.47−1.36 (m, 2H), 1.18−1.14 (m, 6H); ^{13}C NMR (75 MHz, $CDCl_3$) δ: 191.2, 167.3, 152.7, 111.6, 99.1, 70.8, 51.5, 45.2, 41.3, 34.8, 31.2, 27.3, 23.5, 21.6; ESI-MS (*m/z*): 291.2[M+Na]$^+$ (calcd. $C_{14}H_{20}O_5$+Na: 291.3); HRESIMS (*m/z*): 291.1211[M+Na]$^+$ (calcd. $C_{14}H_{20}O_5$+Na: 291.1208).

5.1.2. General procedure for the synthesis of compd. ***8-n*** (*n* = 1–7)

To a 25-mL round-bottom flask, compd. **4-n** (**n** = **1~7**) (0.25 mmol) and compd. **7** (67.1 mg, 0.25 mmol) were dissolved in 10 mL dried methanol. After the addition of 10 mol% amount of activated molecular sieve, the mixture was stirred at r.t. for 4 h. Then the mixture was maintained at 0 °C for 5 min. Afterwards, $NaCNBH_3$ (50.0 mg, 0.75 mmol) was added, and the mixture was kept stirring overnight. To end the reaction, removal of solvent was firstly carried on by rotate evaporation following the addition of saturated NH_4Cl solution. The mixture was then extracted with ethyl acetate (20 mL × 3). All the extractions were combined and washed with saturated NaCl, dried over anhydrous Na_2SO_4. After filtration following removal of solvent, the residues were submitted to RP-HPLC for purification.

5.1.2.1. Methyl (1S,4aS,7S,7aS)-1-isopropoxy-7-(((2-((1,2,3,4-tetrahydroacridin- 9-yl) amino)ethyl)amino)methyl)-1,4a,5,6,7,7a-hexahydrocyclopenta[c]pyran-4- carboxylate (***8-1***).

Compd. **4-1** (60.3 mg, 0.25 mmol) reacted with compd. **7** (67.1 mg, 0.25 mmol) through the procedure described in general procedure. After RP-HPLC purification, 55.5 mg of slight yellow oil **8-1** was obtained in 45% yield. Purity: 97.2%. ^{1}H NMR (300 MHz, $CDCl_3$) δ: 8.20 (t, J = 7.8, 2H), 7.60−7.50 (m, 1H), 7.39−7.28 (m, 2H), 5.33 (d, J = 3.0, 1H), 4.17 (s, 2H), 3.87−3.83 (m, 1H), 3.66 (s, 3H, $-OCH_3$), 3.23−3.18 (m, 2H), 3.06−3.02 (m, 3H), 2.92−2.88 (m, 1H), 2.73-2.46 (m, 4H), 2.33−2.20 (m, 1H), 2.11−2.05 (m, 1H), 1.99-1.61 (m, 6H), 1.54−1.49 (m, 2H), 1.20 (s, 1H), 1.09 (d, J = 6.0, 3H, $-CH_3$), 1.06 (d, J = 6.3, 3H, $-CH_3$); ^{13}C NMR (75 MHz, $CDCl_3$) δ: 167.93, 158.18, 151.75, 151.37, 147.00, 128.41, 128.11, 123.55, 122.97, 120.18, 115.98, 110.74, 97.55, 71.45, 51.18, 50.24, 49.51, 48.17, 43.52, 41.68, 35.68, 33.59, 30.80, 26.95, 24.80, 23.66, 23.01, 22.72, 21.55. HRESIMS (*m/z*): calcd. for $C_{29}H_{40}N_3O_4$ ([M+H]$^+$) 494.2974, found: 494.3013.

5.1.2.2. Methyl (1S,4aS,7S,7aS)-1-isopropoxy-7-(((2-((1,2,3,4-tetrahydroacridin- 9-yl) amino)propyl)amino)methyl)-1,4a,5,6,7,7a-hexahydrocyclopenta[c]pyran-4- carboxylate (***8-2***).

Compd. **4-2** (63.8 mg, 0.25 mmol) reacted with compd. **7** (67.1 mg, 0.25 mmol) through the procedure described in general procedure. After RP-HPLC purification, 60.9 mg of slight yellow oil **8-2** was obtained in 48% yield. Purity: 98.5%. ^{1}H NMR (300 MHz, CD_3OD) δ: 8.15 (d, J = 7.8, 1H), 7.75 (dd, J = 8.4, 0.9, 1H), 7.61−7.56 (m, 1H), 7.48−7.27 (m, 2H), 4.86 (d, J = 9.0, 1H), 4.22−3.93 (m, 1H), 3.78−3.63 (m, 5H), 2.95 (d, J = 5.7, 2H), 2.77−2.69 (m, 6H), 2.58−2.54 (m, 1H), 2.43−2.29 (m, 1H), 2.20−2.14 (m, 1H), 2.01−1.72 (m, 8H), 1.39−1.33 (m, 3H), 1.23−1.10 (m, 7H); ^{13}C NMR (75 MHz, CD_3OD) δ: 168.04, 156.49, 152.24, 151.74, 145.30, 129.01, 125.45, 123.58, 123.28, 119.23, 114.71, 110.41, 97.29, 71.18, 50.31, 48.48, 46.75, 46.61, 42.27, 41.67, 35.56, 32.03, 30.49, 30.06, 26.40, 24.95, 22.70, 22.55, 22.02, 20.56. HRESIMS (*m/z*): calcd. for $C_{30}H_{42}N_3O_4$ ([M+H]$^+$) 508.3131, found: 508.3179.

5.1.2.3. Methyl (1S,4aS,7S,7aS)-1-isopropoxy-7-(((2-((1,2,3,4-tetrahydroacridin- 9-yl) amino)butyl)amino)methyl)-1,4a,5,6,7,7a-hexahydrocyclopenta[c]pyran-4- carboxylate (***8-3***).

Compd. **4-3** (67.3 mg, 0.25 mmol) reacted with compd. **7** (67.1 mg, 0.25 mmol) through the procedure described in general procedure. After RP-HPLC purification, 57.4 mg of slight yellow oil **8-3** was obtained in 44% yield. Purity: 96.6%. ^{1}H NMR (300 MHz, $CDCl_3$) δ: 7.91 (d, J = 8.1, 1H), 7.84 (d, J = 8.1, 1H), 7.49 (t, J = 7.2, 1H), 7.37 (s, 1H), 7.33−7.25 (m, 1H), 4.75 (d, J = 9.0, 1H), 4.05−3.99 (m, 1H), 3.65 (s, 3H, $-OCH_3$), 3.10−2.99 (m, 4H), 2.81−2.75 (m, 1H), 2.70−2.64 (m, 3H), 2.60−2.47 (m, 3H), 2.41−2.29 (m, 1H), 2.27−2.15 (m, 1H), 2.06−2.01 (m, 1H), 1.92−1.76 (m, 6H), 1.72−1.60 (m, 3H), 1.60−1.47 (m, 2H), 1.40−1.26 (m, 2H), 1.19 (d, J = 6.3, 3H, $-CH_3$), 1.15 (d, J = 6.0, 3H, $-CH_3$); ^{13}C NMR (75 MHz, $CDCl_3$) δ: 168.03, 158.41, 151.80,

150.98, 147.28, 128.47, 128.35, 123.69, 122.92, 120.16, 115.85, 110.84, 97.40, 71.22, 51.41, 51.27, 49.62, 49.37, 43.22, 41.59, 35.80, 33.75, 30.80, 29.69, 27.60, 26.92, 24.92, 23.72, 23.07, 22.76, 21.50; HRESIMS (*m/z*): calcd. for $C_{31}H_{44}N_3O_4$ ([M+H]$^+$) 522.3287, found: 522.3326.

*5.1.2.4. Methyl (1S,4aS,7S,7aS)-1-isopropoxy-7-(((2-((1,2,3,4-tetrahydroacridin- 9-yl) amino)pentyl)amino)methyl)-1,4a,5,6,7,7a-hexahydrocyclopenta[c]pyran-4- carboxylate (**8-4**).* Compd. **4-4** (70.8 mg, 0.25 mmol) reacted with compd. **7** (67.1 mg, 0.25 mmol) through the procedure described in general procedure. After RP-HPLC purification, 68.3 mg of slight yellow oil **8-4** was obtained in 51% yield. Purity: 96.2%. ^{1}H NMR (300 MHz, $CDCl_3$) δ: 7.99–7.79 (m, 2H), 7.49 (t, J = 7.5, 1H), 7.36 (s, 1H), 7.28 (t, J = 7.5, 1H), 4.75 (d, J = 9.0, 1H), 4.09–3.99 (m, 2H), 3.64 (s, 3H, $-OCH_3$), 3.13–2.97 (m, 5H), 2.88–2.71 (m, 1H), 2.65–2.58 (m, 3H), 2.56–2.49 (m, 3H), 2.42–2.31 (m, 1H), 2.26–2.14 (m, 1H), 2.06–2.00 (m, 1H), 1.86–1.74 (m, 5H), 1.75–1.55 (m, 2H), 1.52–1.44 (m, 2H), 1.41–1.31 (m, 4H), 1.19 (d, J = 6.3, 3H, $-CH_3$), 1.14 (d, J = 6.0, 3H, $-CH_3$); ^{13}C NMR (75 MHz, $CDCl_3$) δ: 167.90, 157.87, 151.68, 151.14, 146.71, 128.60, 127.91, 123.71, 122.92, 119.83, 115.49, 110.78, 97.33, 71.16, 51.36, 51.17, 49.80, 49.25, 43.07, 41.54, 35.68, 33.44, 31.63, 30.73, 29.76, 26.86, 24.82, 24.71, 23.63, 22.93, 22.57, 21.44. HRESIMS (*m/z*): calcd. for $C_{32}H_{46}N_3O_4$ ([M+H]$^+$) 536.3444, found: 536.3483.

*5.1.2.5. Methyl (1S,4aS,7S,7aS)-1-isopropoxy-7-(((2-((1,2,3,4-tetrahydroacridin- 9-yl) amino)hexyl)amino)methyl)-1,4a,5,6,7,7a-hexahydrocyclopenta[c]pyran-4- carboxylate (**8-5**).* Compd. **4**–**5** (74.4 mg, 0.25 mmol) reacted with compd. **7** (67.1 mg, 0.25 mmol) through the procedure described in general procedure. After RP-HPLC purification, 75.6 mg of slight yellow oil **8-5** was obtained in 55% yield. Purity: 99.3%. ^{1}H NMR (300 MHz, $CDCl_3$) δ: 7.94–7.89 (m, 2H), 7.58–7.49 (m, 1H), 7.41 (s, 1H), 7.37–7.29 (m, 1H), 4.81 (d, J = 9.0, 1H), 4.11–4.04 (m, 1H), 4.03–3.95 (m, 1H), 3.70 (s, 3H, $-OCH_3$), 3.08–3.04 (m, 2H), 2.85–2.81 (m, 1H), 2.75–2.60 (m, 4H), 2.58–2.50 (m, 4H), 2.48–2.35 (m, 1H), 2.31–2.20 (m, 1H), 2.10–2.06 (m, 1H), 1.95–1.80 (m, 6H), 1.72–1.64 (m, 2H), 1.58–1.45 (m, 2H), 1.45–1.32 (m, 6H), 1.25 (d, J = 6.3, 3H, $-CH_3$), 1.20 (d, J = 6.0, 3H, $-CH_3$); ^{13}C NMR (75 MHz, $CDCl_3$) δ: 168.05, 158.38, 151.83, 151.05, 147.34, 128.58, 128.52, 123.76, 123.02, 120.22, 115.87, 110.94, 97.56, 71.31, 51.61, 51.30, 50.15, 49.58, 43.43, 41.68, 35.83, 33.96, 31.84, 30.90, 30.26, 27.43, 27.06, 27.03, 24.88, 23.78, 23.15, 22.85, 21.59. HRESIMS (*m/z*): calcd. for $C_{33}H_{48}N_3O_4$ ([M+H]$^+$) 550.3600, found: 550.3687.

*5.1.2.6. Methyl (1S,4aS,7S,7aS)-1-isopropoxy-7-(((2-((1,2,3,4-tetrahydroacridin- 9-yl) amino)heptyl)amino)methyl)-1,4a,5,6,7,7a-hexahydrocyclopenta[c]pyran-4- carboxylate (**8-6**).* Compd. **4**–**6** (77.7 mg, 0.25 mmol) reacted with compd. **7** (67.1 mg, 0.25 mmol) through the procedure described in general procedure. After RP-HPLC purification, 88.8 mg of slight yellow oil **8-6** was obtained in 63% yield. Purity: 98.7%. ^{1}H NMR (300 MHz, CD_3OD) δ: 8.09 (d, J = 8.4, 1H), 7.77 (d, J = 8.4, 1H), 7.55 (t, J = 7.8, 1H), 7.43 (s, 1H), 7.36 (t, J = 7.5, 1H), 5.00–4.93 (m, 1H), 4.14–4.03 (m, 1H), 3.69 (s, 3H, $-OCH_3$), 3.53 (t, J = 6.9, 2H), 2.97 (s, 2H), 2.89–2.69 (m, 4H), 2.61–2.51 (m, 3H), 2.48–2.41 (m, 1H), 2.28–2.23 (m, 1H), 2.20–1.87 (m, 6H), 1.68–1.58 (m, 2H), 1.49–1.25 (m, 12H), 1.22–1.19 (m, 6H); ^{13}C NMR (75 MHz, CD_3OD) δ: 168.11, 157.49, 151.98, 151.75, 146.33, 128.45, 126.39, 123.32, 123.08, 119.80, 115.24, 110.49, 97.32, 71.16, 50.63, 50.29, 49.10, 48.31, 42.36, 41.72, 35.60, 32.67, 30.82, 30.48, 29.03, 28.89, 26.99, 26.45, 26.38, 24.75, 22.74, 22.70, 22.29, 20.56; HRESIMS (*m/z*): calcd. for $C_{34}H_{50}N_3O_4$ ([M+H]$^+$) 564.3757, found: 564.3823.

*5.1.2.7. Methyl (1S,4aS,7S,7aS)-1-isopropoxy-7-(((2-((1,2,3,4-tetrahydroacridin-9-yl) amino)octyl)amino)methyl)-1,4a,5,6,7,7a-hexahydrocyclopenta[c]pyran-4-carboxylate (**8-7**).* Compd. **4**–**7** (81.4 mg, 0.25 mmol) reacted with compd. **7** (67.1 mg, 0.25 mmol) through the procedure described in general procedure. After RP-HPLC purification, 76.6 mg of slight yellow oil **8-7** was obtained in 53% yield. Purity: 98.5%. ^{1}H NMR (300 MHz, $CDCl_3$) δ: 7.89 (dd, J = 8.4, 0.6, 1H), 7.84 (dd, J = 8.4, 0.6, 1H), 7.50–7.46 (m, 1H), 7.36 (s, 1H), 7.31–7.21 (m, 1H), 4.76 (d, J = 9.0, 1H), 4.10–4.03 (m, 1H), 4.01–3.90 (m, 1H), 3.64 (s, 3H, $-OCH_3$), 3.04–2.96 (m, 2H), 2.80–2.74 (m, 1H), 2.71–2.56 (m, 4H), 2.56–2.42 (m, 3H), 2.38–2.33 (m, 1H), 2.23–2.19 (m, 1H), 2.07–2.03 (m, 1H), 1.91–1.73 (m, 6H), 1.66–1.50 (m, 2H), 1.45–1.38 (m, 2H), 1.37–1.22 (m, 11H), 1.20 (d, J = 6.3, 3H, $-CH_3$), 1.16 (d, J = 6.0, 3H, $-CH_3$); ^{13}C NMR (75 MHz, $CDCl_3$) δ: 167.91, 158.34, 151.69, 150.83, 147.38, 128.57, 128.25, 123.52, 122.87, 120.15, 115.73, 110.78, 97.45, 71.16, 51.47, 51.13, 50.16, 49.49, 43.34, 41.54, 35.68, 33.93, 31.75, 30.76, 30.21, 29.49, 29.28, 27.44, 26.87, 24.75, 23.62, 23.03, 22.75, 21.44. HRESIMS (*m/z*): calcd. for $C_{35}H_{52}N_3O_4$ ([M+H]$^+$) 578.3913, found: 578.3952.

5.2. Cholinesterase inhibition

Acetylcholinesterase (AChE, EC 3.1.1.7) from electric eel (600–800 units/mg, lyophilized powder), Butyrylcholinesterase from equine serum (BuChE, EC 3.1.1.7, min. 500 units/mg protein in buffered aqueous solution), acetylthiocholine iodide (ATCI), *S*-butyrylthiocholine iodide (BTCI), 5, 5′-dithiobis(2-nitrobenzoic acid) (Ellman's reagent, DTNB) and tacrine hydrochloride were purchased from Sigma-Aldrich (St. Louis, MO, USA). The inhibitory activities of test compounds **4-n** (n = 1–7), **7**, and **8-n** (n = 1–7) was evaluated by Ellman's method [47]. The compounds were dissolved in DMSO and diluted with 100 mM phosphate buffer (PBS, pH 8.0) led to corresponding test concentration (DMSO less than 0.01%). In each well of the plate, 150 μl of PBS, 10 μl of 10 mM DTNB, 20 μl of AChE (1.0 U/ml) or 20 μl of BuChE (1.0 U/ml) were incubated with 10 μL of different concentrations of tested compounds (1.0–100 μM) at 37 °C for 6 min. After this period, ATCI (10 mM) or BTCI (10 mM) as the substrate (10 μL) was added and the absorbance was measured with a wavelength of 412 nm at a frequency of once per 10 s within 1 min. IC_{50} values were calculated as concentration of compound that produces 50% enzyme activity inhibition, using the Graph Pad Prism 4.03 software (San Diego, CA, USA). Results are expressed as the mean ± SD of at least three different experiments performed in triplicate.

5.3. Cell culture

Human neuroblastoma SH-SY5Y cells were cultured in DMEM medium containing 10% (v/v) fetal bovine serum (FBS), 100 μg/mL of streptomycin and 100 U/ml of penicillin in a water-jacketed incubator at 37 °C in a humidified atmosphere of 5% CO_2. Cells were fed every 3 days and sub-cultured once they reached 80–90% confluence.

5.4. MTT assay

The viability of SH-SY5Y cells mediated by drugs was measured using 3-(4,5-dimethylthiazol-2-yl)-2,5-diphenyltetrazolium bromide (MTT, 570 nm) assay. The process was described below: Cells in suspension were plated in 96-well plates at a density of 5×10^3 cells/well and were treated with either vehicle (0.1% DMSO) or drugs for 4 h after 24 h culture. The final DMSO concentration in all experiments was less than 0.1% in medium. The medium was discharged and the cells were washed with PBS. Cells were treated

with 35 mM glutamic acid for 24 h. Again, the medium was discharged and the cells were washed with PBS. Then 10 μL 5 mg/mL MTT solutions were added to each well, and the plate was incubated for an additional 4 h. The absorbance was measured at 570 nm using a microplate reader (Bio-Rad; Hercules, CA, USA) after 150 μL of DMSO added. All of the tests were repeated at least 3 times.

5.5. Nitrite measurement in vitro

The levels of intracellular NO were determined by the colorimetric assay using the nitrite colorimetric assay kit (Beyotime, China), according to the manufacturer's instructions. Briefly, SH-SY5Y cells (2×10^5 cells/well) were treated with either vehicle (0.1% DMSO) or drugs for 4 h after 24 h culture. The final DMSO concentration in all experiments was less than 0.1% in medium. The medium was discharged and the cells were washed with PBS. Cells were treated with 35 mM glutamic acid for 24 h. Again, the medium was discharged and the cells were washed with PBS. Subsequently, the cells were harvested and their cell lysates were prepared and then mixed with Griess reagent for 10 min at 37 °C, followed by measurement at 540 nm by a microplate reader. The cells treated with 0.4% DMSO in medium were used as negative controls for the background levels of nitrite production, while sodium nitrite at different concentrations was prepared as the positive control for the establishment of a standard curve. Each experiment was repeated at least three times.

5.6. Measurement of intracellular Ca^{2+} ($[Ca^{2+}]_i$)

$[Ca^{2+}]_i$ was monitored using the fluorescent Ca^{2+}-sensitive dye, Fura-3-acetoxymethy ester (Fura-3-AM). SH-SY5Y cells in the exponential phase were plated on a 96-well cell culture plate with 2×10^3 cells/well treated with either vehicle (0.1% DMSO) or drugs for 4 h after 24 h culture. Cells were treated with 35 mM glutamic acid for another 24 h. Briefly, cells were trypsinized, pelleted, resuspended in medium and incubated with 5 μM Fura-3-AM in PBS containing 1.3 mM $CaCl_2$ for 40 min at 37 °C and then washed twice to remove any extracellular dye. All the dyed cells were submitted to a flow cytometry (BD FACS Calibur, Franklin Lakes, CA, USA) for fluorescence detection. Excitation wavelength was 340/380 nm; emission wavelength was 510 nm. The fluorescence ratio (F340/F380) was calculated as an indicator of $[Ca^{2+}]_i$.

5.7. Western blotting analysis

SH-SY5Y cells were collected and washed with PBS after the treatment followed the procedure as described above. Then, the cells were lysed with RIPA buffer for 45 min on ice and then centrifuged at 12,000 g at 4 °C for 15 min. Afterwards, the protein content of the supernatant was determined with a Pierce BCA protein assay kit (Thermo Fisher Scientific, USA) to ensure equal sample loading. Protein lysates were separated in 12% SDS-PAGE and blotted onto nitrocellulose membranes (Amersham Biosciences, USA). Proteins were detected using the primary monoclonal antibody of β-Actin (1:3000), AChE (1:1000), BACE1 (1:2000), *i*-NOS (1:500), Caspase 3 (1:1000), Cleaved Caspase 3 (1:1000), p53 (1:3000), Bcl-2 (1:1000), Bax (1:1000), LC3 (1:1000), p62 (1:1000), Aβ (1:2000) with the corresponding diluted ratio given in parentheses, respectively for at least 16 h at 4 °C, and then washed and incubated with HRP-conjugated secondary antibodies at room temperature for 1 h. Protein bands were visualized using enhanced chemiluminescence detection reagents (Bio-Rad, USA). The resulting images were scanned using a scanner (Epson V330 Photo, Japan).

5.8. BBB permeation assay

The BBB penetration of compounds was evaluated using the parallel artificial membrane permeation assay (PAMPA) described by Di et al. [41]. Commercial drugs were purchased from Sigma and Alfa Aesar. Porcine brain lipid (PBL) was obtained from Avanti Polar Lipids. The donor microplate (PVDF membrane, pore size 0.45 mm) and acceptor microplate were both from Millipore. The 96-well UV plate (COSTAR) was from Corning Incorporated. The acceptor 96-well microplate was filled with 300 μL PBS/EtOH (7:3), and the filter membrane was impregnated with 4 μL PBL in dodecane (20 mg/mL). Compounds were dissolved in DMSO at 5 mg/mL and diluted 50-fold in PBS/EtOH (7:3) to a final concentration of 100 μg/mL. Then, 200 μL of the solution was added to the donor wells. The acceptor filter plate was carefully placed on the donor plate to form a sandwich, which was left undisturbed for 10 h at 25 °C. After incubation, the donor plate was carefully removed, and the concentration of compounds in the acceptor wells was determined using the UV plate reader (Flexstation 3). Every sample was analyzed at five wavelengths in four wells and in at least three independent runs. P_e was calculated by the following expression: $P_e = -V_d \times V_a/[(V_d + V_a)A \times t] \times \ln(1 - \text{drug}_{\text{acceptor}}/\text{drug}_{\text{equilibrium}})$, where V_d is the volume of donor well; V_a, volume in acceptor well; A, filter area; t, permeation time; $\text{drug}_{\text{acceptor}}$, the absorbance obtained in the acceptor well; and $\text{drug}_{\text{equilibrium}}$, the theoretical equilibrium absorbance. The results are given as the mean ± standard deviation. In the experiment, 7 quality control standards (Table S1) of known BBB permeability were included to validate the analysis set. A plot of the experimental data versus literature values gave a strong linear correlation, P_e (exp.) = 1.1719P_e (lit.) − 0.0221 ($R^2 = 0.9404$) (Figure S6). From this equation and the limit established by Di et al. (P_e (lit.) = 4.0×10^{-6} cm/s) for BBB permeation, we concluded that compounds with a permeability > 4.67×10^{-6} cm/s could cross the BBB (Table S2).

5.9. Statistical analysis

Experimental values were given as means ± SD. Statistical analysis of the data was performed using the SPSS 18.0 statistical software. One-way analysis of variance (ANOVA) was applied to analyze for difference in data of biochemical parameters among the different groups, followed by Dunnett's significant post-hoc test for pairwise multiple comparisons. Differences were considered as statistically significant at $^*P < 0.05$, $^{**}P < 0.01$.

Declaration of competing interest

The authors declare that they have no known competing financial interests or personal relationships that could have appeared to influence the work reported in this paper.

Acknowledgments

This research was financially supported by National Natural Science Foundation of China (Nos. 81172982 and 81973190), Guangdong Provincial Natural Science Foundation projects (2018B030311020 and 2020A1515010857). The authors will give heartful thanks to Prof. Dr. Hiroshi Kurihara and Prof. Dr. Rongrong He for their equipment support and useful discussion.

Appendix A. Supplementary data

Supplementary data to this article can be found online at https://doi.org/10.1016/j.ejmech.2020.113067.

References

[1] Y. Huang, L. Mucke, Alzheimer mechanisms and therapeutic strategies, Cell 148 (2012) 1204–1222.
[2] M. Vaz, S. Silvestre, Alzheimer's disease: recent treatment strategies, Eur. J. Pharmacol. 887 (2020) 173554.
[3] H.F. Kung, The beta-amyloid hypothesis in Alzheimer's disease: seeing is believing, ACS Med. Chem. Lett. 3 (2012) 265–267.
[4] S. Muralidar, S.V. Ambi, S. Sekaran, D. Thirumalai, B. Palaniappan, Role of tau protein in Alzheimer's disease: the prime pathological player, Int. J. Biol. Macromol. 163 (2020) 1599–1617.
[5] M. Calvo-Rodriguez, B.J. Bacskail, High mitochondrial calcium levels precede neuronal death in vivo in Alzheimer's disease, Cell Stress 4 (2020) 187–190.
[6] C.S. Chan, T.S. Gertler, D.J. Surmeier, Calcium homeostasis, selective vulnerability and Parkinson's disease, Trends Neurosci. 32 (2009) 249–256.
[7] N.C. Inestrosa, A. Alvarez, C.A. Pérez, R.D. Moreno, M. Vicente, C. Linker, O.I. Casanueva, C. Soto, J. Garrido, Acetylcholinesterase accelerates assembly of amyloid- beta-peptides into Alzheimer's fibrils: possible role of the peripheral site of the enzyme, Neuron 16 (1996) 881–891.
[8] C. Haass, D.J. Selkoe, Soluble protein oligomers in neurodegeneration: lessons from the Alzheimer's amyloid beta-peptide, Nat. Rev. Mol. Cell Biol. 8 (2007) 101–112.
[9] P. Csermely, V. Agoston, S. Pongor, The efficiency of multi-target drugs: the network approach might help drug design, Trends Pharmacol. Sci. 26 (2005) 178–182.
[10] R. Morphy, Z. Rankovic, Designed multiple ligands. An emerging drug discovery paradigm, J. Med. Chem. 48 (2005) 6523–6543.
[11] R. Morphy, Z. Rankovic, Fragments, network biology and designing multiple ligands, Drug Discov. Today 12 (2007) 156–160.
[12] A. Cavalli, M.L. Bolognesi, A. Minarini, M. Rosini, V. Tumiatti, M. Recanatini, C. Melchiorre, Multi-target-Directed ligands to combat neurodegenerative diseases, J. Med. Chem. 51 (2008) 347–372.
[13] C.J. Van der Schyf, W.J. Geldenhuys, M.B. Youdim, Multifunctional drugs with different CNS targets for neuropsychiatric disorders, J. Neurochem. 99 (2006) 1033–1048.
[14] A. Minarini, A. Milelli, E. Simoni, M. Rosini, M.L. Bolognesi, C. Marchetti, V. Tumiatti, Multifunctional tacrine derivatives in Alzheimer's disease, Curr. Top. Med. Chem. 13 (2013) 1771–1786.
[15] R.A. de Aquino, L.V. Modolo, R.B. Alves, A. de Fatima, Design of new drugs for the treatment of Alzheimer's disease based on tacrine structure, Curr. Drug Targets 14 (2013) 378–397.
[16] M.I. Fernandez-Bachiller, C. Perez, L. Monjas, J. Rademann, M.I. Rodriguez-Franco, New tacrine-4-oxo-4H-chromene hybrids as multifunctional agents for the treatment of Alzheimer's disease, with cholinergic, antioxidant, and beta-amyloid-reducing properties, J. Med. Chem. 55 (2012) 1303–1307.
[17] L. Wang, G. Esteban, M. Ojima, O.M. Bautista-Aguilera, T. Inokuchi, I. Moraleda, I. Iriepa, A. Samadi, M.B.H. Youdim, A. Romero, E. Soriano, R. Herrero, A.P. Fernández, Ricardo-Martínez-Murillo, J. Marco-Contelles, M. Unzeta, Donepezil plus propargyl- amine+8-hydroxyquinoline hybrids as new multifunctional metal-chelators, AChE and MAO inhibitors for the potential treatment of Alzheimer's disease, Eur. J. Med. Chem. 80 (2014) 543–561.
[18] K. Chalupova, J. Korabecny, M. Bartolini, et al., Novel tacrine-tryptophan hybrids: multi-target directed ligands as potential treatment for Alzheimer's disease, Eur. J. Med. Chem. 168 (2019) 491–514.
[19] Q. Meng, J. Ru, G. Zhang, C. Shen, S. Schmitmeier, A. Bader, Re-evaluation of tacrine hepatotoxicity using gel entrapped hepatocytes, Toxicol. Lett. 168 (2007) 140–147.
[20] P. Dogterom, J.F. Nagelkerke, G.J. Mulder, Hepatotoxicity of tetrahydroaminoacridine in isolated rat hepatocytes: effect of glutathione and vitamin E, Biochem. Pharmacol. 37 (1988) 2311–2313.
[21] S. Xie, J. Lan, X. Wang, N. Jiang, G. Dong, Z. Li, K.D.G. Wang, P. Guo, L. Kong, Multifunctional tacrine-trolox hybrids for the treatment of Alzheimer's disease with cholinergic, antioxidant, neuroprotective and hepatoprotective properties, Eur. J. Med. Chem. 93 (2015) 42–50.
[22] J. Hardy, D.J. Selkoe, The amyloid hypothesis of Alzheimer's disease: progress and problems on the road to therapeutics, Science 297 (2002) 353–356.
[23] P. Nilsson, K. Loganathan, M. Sekiguchi, Y. Matsuba, K. Hui, S. Tsubuki, M. Tanaka, N. Iwata, T. Saito, T.C. Saido, Aβ secretion and plaque formation depend on autophagy, Cell Rep. 5 (2013) 61–69.
[24] J. Luo, R. Wang, Z. Huang, J. Yang, X. Yao, H. Chen, W. Zheng, Synthesis of stable derivatives from genipin and studies of their neuroprotective activity in PC12 cells, ChemMedChem 7 (2012) 1661–1668.
[25] R. Wang, J. Yang, S. Liao, G. Xiao, J. Luo, L. Zhang, P.J. Little, H. Chen, W. Zheng, Stereoselective reduction of 1-*O*-isopropyloxygenipin enhances its neuroprotective activity in neuronal cells from apoptosis induced by sodium nitroprusside, ChemMedChem 9 (2014) 1397–1401.
[26] R. Wang, J. Zhao, L. Zhang, L. Peng, X. Zhang, W. Zheng, H. Chen, Genipin derivatives protect RGC-5 from sodium nitroprusside-induced nitrosative stress, Int. J. Mol. Sci. 17 (2016) 117, https://doi.org/10.3390/ijms.17010117.
[27] J. Zhao, L. Peng, W. Zheng, R. Wang, L. Zhang, X. Zhang, J. Yang, H. Chen, Chemically bonding of amantadine with gardenamide A enhances the neuroprotective effects against corticosterone-induced insults in PC12 cells, Int. J. Mol. Sci. 16 (9) (2015) 22795–22810, https://doi.org/10.3390/ijms160922795.
[28] Y. Koriyama, K. Chiba, M. Yamazaki, H. Suzuki, K. Muramoto, S. Kato, Long-acting genipin derivative protects retinal ganglion cells from oxidative stress models *in vitro* and *in vivo* through the Nrf2/antioxidant response element signaling pathway, J. Neurochem. 115 (2010) 79–91.
[29] Y. Koriyama, Y. Takagi, K. Chiba, M. Yamazaki, K. Arai, T. Matsukawa, H. Suzuki, K. Sugitani, H. Kagechika, S. Kato, Neuritogenic activity of a genipin derivative in retinal ganglion cells is mediated by retinoic acid receptor beta expression through nitric oxide/S-nitrosylation signaling, J. Neurochem. 119 (2011) 1232–1242.
[30] S. Sarkar, V.I. Korolchuk, M. Renna, S. Imarisio, A. Fleming, A. Williams, M. Garcia-Arencibia, C. Rose, S. Luo, B.R. Underwood, G. Kroemer, C.J. O'Kane, D.C. Rubinsztein, Complex inhibitory effects of nitric oxide on autophagy, Mol. Cell. 43 (2011) 19–32.
[31] P.R. Carlier, E.S.-H. Chow, Y. Han, J. Liu, J. El Yazal, Y.-P. Pang, Heterodimeric tacrine-based acetylcholinesterase inhibitors: investigating ligand peripheral site interactions, J. Med. Chem. 42 (1999) 4225–4231.
[32] M. Rosini, V. Andrisano, M. Bartolini, M.L. Bolognesi, P. Hrelia, A. Minarini, A. Tarozzi, C. Melchiorre, Rational approach to discover multipotent anti-alzheimer drugs, J. Med. Chem. 48 (2) (2005) 360–363.
[33] L. Fang, B. Kraus, J. Lehmann, J. Heilmann, Y. Zhang, M. Decker, Design and synthesis of tacrine–ferulic acid hybrids as multi-potent anti-Alzheimer drug candidates, Bioorg. Med. Chem. Lett 18 (2008) 2905–2909.
[34] S.M. Hague, S. Klaffke, O. Bandmann, Neurodegenerative disorders: Parkinson's disease and Huntington's disease, J. Neurol. Neurosurg. Psychiatry 76 (2005) 1058–1063.
[35] K. Parameshwaran, M. Dhanasekaran, V. Suppiramaniam, Amyloid beta peptides and glutamatergic synaptic dysregulation, Exp. Neurol. 210 (2008) 7–13.
[36] X. Dong, Y. Wang, Z. Qin, Molecular mechanisms of excitotoxicity and their relevance to pathogenesis of neurodegenerative diseases, Acta Pharmacol. Sin. 30 (4) (2009) 379–387.
[37] L.K. Friedman, Calcium: a role for neuroprotection and sustained adaptation, Mol. Interv. 6 (2006) 315–329.
[38] S.R. Robinson, G.M. Bishop, Aß as a bioflocculant: implications for the amyloid hypothesis of Alzheimer's disease, Neurobiol Ageing 23 (2002) 1051–1072.
[39] P.C. Wong, H. Cai, D.R. Borchelt, D.L. Price, Genetically engineered mouse models of neurodegenerative diseases, Nat. Neurosci. 5 (2002) 633–639.
[40] I. Kim, S. Rodriguez-Enriquez, J.J. Lemasters, Selective degradation of mitochondria by mitophagy, Arch. Biochem. Biophys. 462 (2007) 245–253.
[41] L. Di, E.H. Kerns, K. Fan, O.J. McConnell, G.T. Carter, High throughput artificial membrane permeability assay for blood-brain barrier, Eur. J. Med. Chem. 38 (2003) 223–232.
[42] R. Schliebs, T. Arendt, The significance of the cholinergic system in the brain during aging and in Alzheimer's disease, J. Neural. Transm. 113 (2006) 1625–1644.
[43] W.L. Klein, G.A. Krafft, C.E. Finch, Targeting small abeta oligomers: the solution to an Alzheimer's disease conundrum? Trends Neurosci. 24 (2001) 219–224.
[44] J. Hardy, D.J. Selkoe, The amyloid hypothesis of Alzheimer's disease: progress and problems on the road to therapeutics, Science 297 (2002) 353–356.
[45] R.A. Nixon, The role of autophagy in neurodegenerative disease, Nat. Med. 19 (8) (2013) 983–997.
[46] X. Zhang, S. Yuan, J. Zhao, L. Zhang, C. Zhang, R. Wang, H. Chen, Design synthesis of gardenamide A/tacrine hybrids and their protection against 6-Hydroxydopamine-induced insults in PC12 cells, chin, J. Org. Chem. 37 (2017) 873–880.
[47] G.L. Ellman, K.D. Courteney, V. Andres Jr., R.M. Feather-Stone, A new and rapid colorimetric determination of acetylcholinesterase activity, Biochem. Pharmacol. 7 (1961) 88–95.